The direct influence of the support on the electronic structure of the active sites in supported metal catalysts: evidence from Pt–H anti-bonding shape resonance and Pt–CO FTIR data

D.C. Koningsberger [a,*], D.E. Ramaker [b], J.T. Miller [c], J. de Graaf [a] and B.L. Mojet [a,**]

[a] *Department of Inorganic Chemistry and Catalysis, Debye Institute, Utrecht University, PO Box 80083, 3508 TB Utrecht, The Netherlands*
[b] *Department of Chemistry and Material Science Institute, George Washington Unversity, Washington DC, USA*
[c] *Amoco Research Center, E-1F, 150 W Warrenville RD, Naperville, IL 606563, USA*

The catalytic activity and spectroscopic properties of supported noble metal catalysts are strongly influenced by support properties such as the presence of protons, type of charge compensating cations, Si/Al ratio and/or presence of extra-framework Al. The metal–support interaction is relatively independent of the metal (Pd or Pt) or the type of support (microporous zeolites such as LTL and Y or macroporous supports such as SiO_2). As the alkalinity of the support increases (i.e., with increasing electronic charge on the support oxygen ions), the TOF of the metal particles for neopentane hydrogenolysis decreases. At the same time, there is a systematic shift from linear to bridge bonded CO as indicated by the IR spectra. This is a strong indication of a change in the electronic structure of the catalytically active Pt surface atoms. Analysis of the Pt–H anti-bonding shape resonance present in the Pt X-ray absorption spectra of the L_3 edge indicates that the difference in energy between the Pt–H anti-bonding orbital and the Fermi level decreases as the alkalinity of the support increases. The results from the IR and Pt–H shape resonance data directly show that the support influences the position in energy of the metal valence orbitals. The ionisation potential of the catalytically active Pt surface atoms decreases with increasing support alkalinity, i.e., with increasing electron charge on the support oxygen ions. This shift leads to a weakening of the Pt–H bond.

KEY WORDS: XAFS spectroscopy; Pt–H anti-bonding shape resonance; metal–support interaction; Pt–H bonding; FTIR of chemisorbed CO; TOF of neopentane hydrogenolysis; support alkalinity; Pt/SiO_2; Pt and Pd/LTL; Pt/Y

1. Introduction

The mechanism of the metal–support interaction and more precisely how the electronic structure of the catalytically active surface metal atoms is altered by the support is still unresolved in the literature. However, the effects of the metal–support interaction on the catalytic properties of noble metal particles have been found and discussed by many authors [1–8]. The formation of a metal–proton adduct has been proposed to account for electron-deficient metal particles [9]. The electron deficiency was derived from XPS data collected on Pd metal particles dispersed in acidic zeolites [10]. The proton was proposed to be delocalised over the metal particle thereby withdrawing electron density from the surface atoms. However, such adducts cannot account for an increase in electron density for metal particles on alkaline supports. In another model the electronegativity of the support oxygen atoms was suggested to decrease with increasing zeolite alkalinity [11–13]. Charge transfer between the support oxygen atoms and the close by metal particles was thought to cause higher electron density on the metal particles in alkaline zeolites. A third model is based on the polarisation of a small metal cluster by nearby cations [14,15]. Calculations indicated that metal atoms near cations attract electrons, thus resulting in electron-deficient metal atoms situated at the opposite side of the cluster. In this model, there is no net change in electron density of the cluster. To understand the interaction involved, we have reported on the effect of the support on (i) the atomic XAFS spectra and (ii) the X-ray absorption edge of very small platinum particles dispersed in LTL [16] and Y [17] zeolite. The X-ray absorption edges of the supported Pt particles were measured with and without adsorbed hydrogen, a reactant used in many catalytic reactions. The results show a direct influence of the support on the electronic structure of the supported platinum particles.

This paper summarises the reaction rates for neopentane hydrogenolysis catalysed by Pt and Pt particles supported on SiO_2, LTL and Y zeolite. The support has been varied by changing the number of protons, type of charge compensating cations, Si/Al ratio and/or presence of extra-framework Al in order to alter the catalytic properties of the metal particles. The change in the electronic properties has been investigated using FTIR of chemisorbed CO (Pt and Pd) and a recently developed analysis method [18] of the Pt L_3 and L_2 X-ray absorption edges. The analysis method isolates the Pt–H anti-bonding shape resonance state present above the Fermi level at the L_3 edge. The Pt–H anti-bonding state is created by chemisorption of hydrogen on the surface atoms of the platinum particles. The results of FTIR can be interpreted in terms of a decrease in ionisation potential of the valence d-orbitals with increasing alkalinity of the support oxygen ions. The simultaneous decrease in energy with re-

* To whom correspondence should be addressed.
** Current address: Schuit Institute of Catalysis, Eindhoven University of Technology, PO Box 523, 5600 MB Eindhoven, The Netherlands.

1022-5528/01/0100-0035$18.00/0

spect to the Fermi level (E_{res}) of the Pt–H anti-bonding state implies a decrease in the strength of the Pt–H bond.

2. Experimental

2.1. Catalyst preparation

Details of the preparation of all catalysts are given in [16, 17]. The acidity/alkalinity of the LTL zeolite supports was varied by either impregnating a commercial K-LTL zeolite with KNO_3 or exchanging with NH_4NO_3 to give K/Al ratios ranging from 0.55 to 1.45 for Pd/LTL and from 0.63 to 1.25 for Pt/LTL. Palladium and platinum were added using aqueous solutions of $(Pd(NH_3)_4)(NO_3)_2$ and $(Pt(NH_3)_4)(NO_3)_2$. The catalysts are designated Pt/LTL(x) or Pd/LTL(x) with x representing the K/Al molar ratio.

The basic silica supports were prepared by ion-exchange of SiO_2 with increasing amounts of KOH. Also, an acidic silica was prepared by ion-exchange of SiO_2 with excess $Al(NO_3)_3$. Platinum was added using an aqueous solution of $(Pt(NH_3)_4)(NO_3)_2$. The catalysts are designated Pt/SiO_2–X (*.**) with X representing Al or K and (*.**) the wt% of X.

NaY (LZY-54, UOP) was ion-exchanged with $La(NO_3)_3$ or NH_4NO_3. H-USY (LZY-84, UOP) was ion-exchanged with excess KNO_3 to obtain K-USY. Platinum was added to each support by ion-exchange with $[Pt(NH_3)_4](NO_3)_2$ at 80 °C. The resulting catalysts are denoted by Pt/NaY, Pt/NaLaY, Pt/H-NaY, Pt/K-USY and Pt/H-USY.

The Pt dispersion was determined by hydrogen chemisorption [16,17] and for the Pt/Y catalysts the number of acid sites was determined by TPD of chemisorbed NH_3 [17].

2.2. Neopentane hydrogenolysis

Neopentane hydrogenolysis was conducted in a fixed-bed reactor at 250 °C, using 0.99 vol% neopentane in H_2. The catalysts were pre-reduced and conversion was adjusted to values between 0.5 and 2.0% by varying space velocity. The initial conversion and selectivity were determined by extrapolation to time zero. The TOF (at time zero) was calculated based on H_2 chemisorption. Selectivities were calculated on a molar basis as the percent of neopentane converted to isopentane (isomerisation) and isobutane plus methane (hydrogenolysis) extrapolated to zero conversion and deactivation. The analysis of the reaction products was carried out using the Delplot method [19], which gives by extrapolation to zero conversion the primary product distribution.

2.3. Infrared spectroscopy

Transmission infrared spectra were recorded on a Perkin–Elmer 1720-X Fourier transform spectrometer at a spectral resolution of 4 cm^{-1}. The catalysts were pressed in thin self-supporting wafers and placed in an *in situ* transmission infrared cell provided with CaF_2 windows [21]. Each catalyst was dried at 120 °C, reduced in H_2 at 300 °C and cooled to room temperature under H_2 atmosphere, except for Pd/LTL samples that were cooled in He to avoid formation of palladium hydrides. Subsequently at room temperature, the sample was purged with He for 10 min followed by flowing 20% CO in He gas at atmospheric pressure for 10 min, after which the CO absorbance spectrum was collected at room temperature. The spectra for Pd/LTL and Pt/LTL were collected under wet conditions to prevent the ion–dipole interaction between zeolite cations and adsorbed CO [20]. The spectra were corrected for the infrared adsorption of the specific support material and gas phase CO.

2.4. XAFS data collection and data analysis

The X-ray absorption spectra of the Pt L_3 and L_2 edge were taken at the SRS (Daresbury) Wiggler Station 9.2, using a Si(220) double crystal monochromator. Samples were pressed into self-supporting wafers (calculated to have an absorbance of 2.5) and placed in a controlled atmosphere cell [21]. All spectra were recorded at liquid nitrogen temperature. The Pt/LTL samples were reduced in H_2 at 300 °C and subsequent treatment in a helium flow for 1 h at 300 °C to remove chemisorbed hydrogen. The EXAFS samples Pt/NaY and Pt/H-USY were reduced in flowing hydrogen at 400 °C (heating rate 5 °C/min) for 1 h. Subsequently, the samples were evacuated at 200 °C for 1 h and XAFS spectra were recorded at liquid nitrogen temperature maintaining a vacuum of better than 2×10^{-5} Pa. Samples with chemisorbed hydrogen further denoted by H–Pt; samples after treatment in He or in vacuation further denoted by Pt.

The final XAFS spectrum was obtained by averaging 3–4 scans. The absorption data was background subtracted using standard procedures. The pre-edge background was approximated by a modified Victoreen and removed from the raw data. The post-edge background was removed using a cubic-spline approximation [22] and the spectra were normalised on the absorption edge step height at 50 eV past the absorption edge.

2.5. Pt–H anti-bonding shape resonance

Recently, it has been shown that analysis of a shape resonance in the XANES spectra for noble metal catalysts gives direct information on the changes in the nature of the bonding between chemisorbed hydrogen and the metal cluster [18]. The partially occupied platinum surface d-orbitals interact with the hydrogen 1s orbital producing bonding and anti-bonding Pt–H orbitals [23] (see figure 1). The Pt–H bonding orbital is primarily localised on the H atom, and the anti-bonding state (AS) is localised more on the surface Pt atoms. The $5d_{3/2}$ component (reflected in the L_2 edge) of the AS state is assumed to exist below the Fermi level along with the rest of the $5d_{3/2}$ band. However, the excitation of the photoelectron into the empty $5d_{5/2}$ component of the AS state should be evident at the L_3 X-ray absorption edge. The bonding orbital is occupied in both cases and thus is not visible by XAFS.

The empty anti-bonding orbital (AS) can be isolated by subtraction of the Pt L_3 and L_2 near edge spectra with (Pt–H)

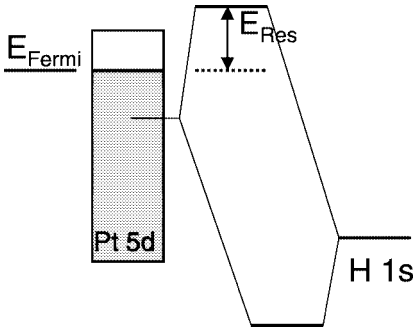

Figure 1. Molecular orbital (MO) picture showing formation of bonding and anti-bonding orbitals derived from a surface Pt orbital and the H 1s orbital (see also [23]).

and without chemisorbed hydrogen (Pt). A full description has been given elsewhere [18]. Briefly, both L_2 edges were aligned at 0.6 step height, whereas both the L_3(Pt/LTL) and the L_3(He–Pt/LTL) edges were aligned relative to the comparable L_2 edges with the help of the EXAFS oscillations.

The anti-bonding state can be viewed as a localised state degenerate with a continuum state, here described by the Pt–H EXAFS final state wave function. The outgoing electron will reside temporarily in the potential well determined by the AS state and can escape undergoing a resonance with the Pt–H EXAFS final state wave function. This one electron process causes a shape resonance with the well-known Fano-like resonance line shape. Its effect on the scattering cross section $\sigma(E)$ can be related to an EXAFS function $\chi(E)$ via the normal expression $\sigma(E) = \mu(E)(1 + \chi(E))$. It can be shown [18] that

$$\chi(E) = A \sin\Phi\big[(1 - q\varepsilon)/\big(1 + \varepsilon^2\big)\big], \qquad (1)$$

where A an amplitude factor, $q = \cot\Phi$ and $\varepsilon = 2(E - E_{\mathrm{res}})/\Gamma$. Φ can be related to the usual total phase found in EXAFS containing the $2kr$ term and the phase from the absorber and back-scatterer. ε is the normalised energy scale relative to the resonance energy (E_{res}), whereby Γ represents the resonance width. A fit to the experimentally observed AS lineshape gives values for E_{res}, Γ, A and Φ. The AS data described in this paper were fitted using an expression for the phase Φ as derived and discussed in [24].

3. Results

3.1. Neopentane hydrogenolysis

In figure 2 the turnover frequencies (TOF) for neopentane hydrogenolysis on Pt and Pd particles supported on both zeolite LTL and amorphous SiO_2 are plotted as a function of the support alkalinity. There is a continuous decrease in the TOF from 10^{-3} to 10^{-5} as the alkalinity of the support increases from acidic to neutral to alkaline with increasing amounts of potassium. The results obtained for the Pt/Y catalysts are given in table 1. The number of protons for the different Pt/Y catalysts as determined form NH_3 TPD is also given in table 1. Table 2 allows a more detailed analysis of the influence of the different support properties as reflected in the number of protons, cation charge, Si/Al ratio and extra-framework Al (Al_{EF}). The TOF for neopentane hydrogenolysis increases with larger number of protons, with increasing charge of cations and with increasing Si/Al ratio and/or presence of Al_{EF}. The results show that the support properties directly determine the TOF for neopentane hydrogenolysis catalysed by Pt and Pd particles.

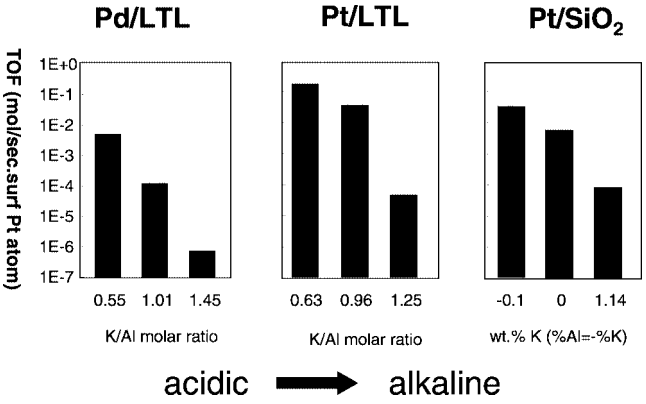

Figure 2. TOF of neopentane hydrogenolysis as a function of the support alkalinity for Pd/LTL, Pt/LTL and Pt/SiO_2.

Table 1
Number of acid sites and turnover frequency of neopentane by Pt/Y catalysts.

Catalyst	Acid sites (mmol/g)	TOF[a]
Pt/NaY	0.15	5.9×10^{-5}
Pt/H-NaY	1.96	5.0×10^{-4}
Pt/K-USY	0.16	1.2×10^{-3}
Pt/H-USY	1.61	7.7×10^{-3}
Pt/NaLaY (2%)	0.22	1.5×10^{-3}

[a] TOF (molecules/s surface-Pt-atom) determined at 250 °C, 1 atm and with 1% neopentane in H_2.

Table 2
Effect of protons, cation charge, Si/Al ratio and/or extra-framework Al (Al_{EF}) on TOF.

Effect	Pt/NaY	Pt/H–NaY	Pt/NaLaY	Pt/K-USY	Pt/H-USY
Protons	1	8.5		1	6.5
Cation charge	1		25.4		
Si/Al and/or Al_{EF}	1	1		20	15.4

3.2. FTIR of chemisorbed CO

An example of the transmission infrared spectra of chemisorbed CO on Pd/LTL is given in figure 3. These spectra are typical for Pd or Pt particles supported on zeolite LTL or SiO_2 [25,26]. Two regions of adsorbed CO can be assigned: at higher wavenumbers an adsorption band due to linearly co-ordinated CO, and at lower wavenumbers adsorption due to CO in bridged co-ordination. Both adsorption bands shift to lower wavenumbers as the sup-

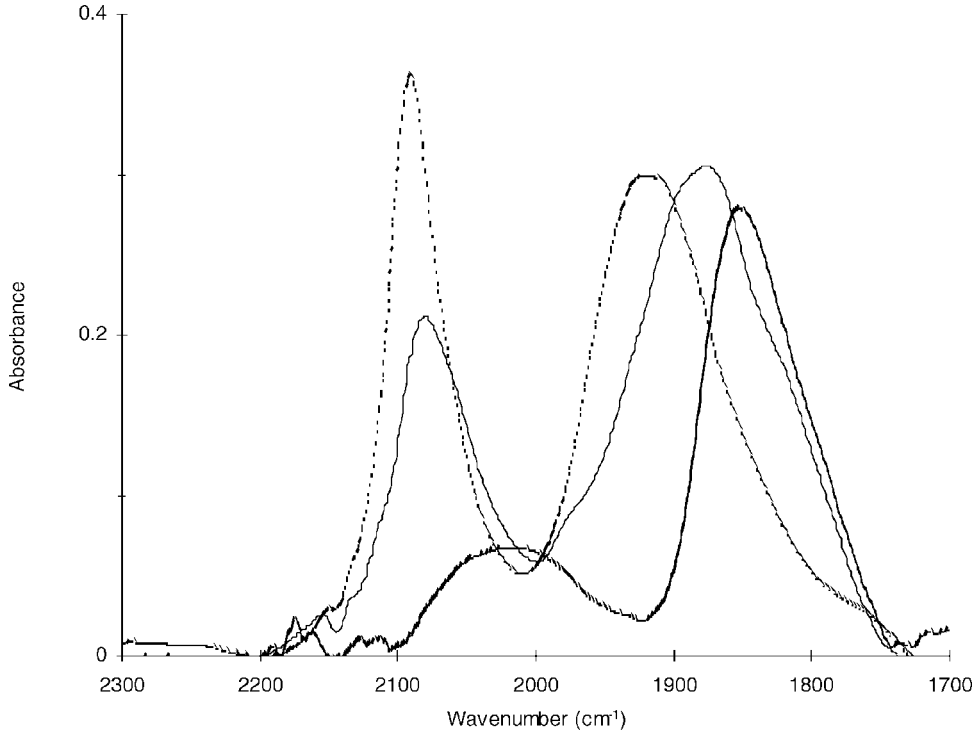

Figure 3. FTIR spectra taken under wet conditions at 1 atm CO pressure for Pd/LTL(0.55) (···), Pd/LTL(1.01) (—) and Pd/LTL(1.45) (—).

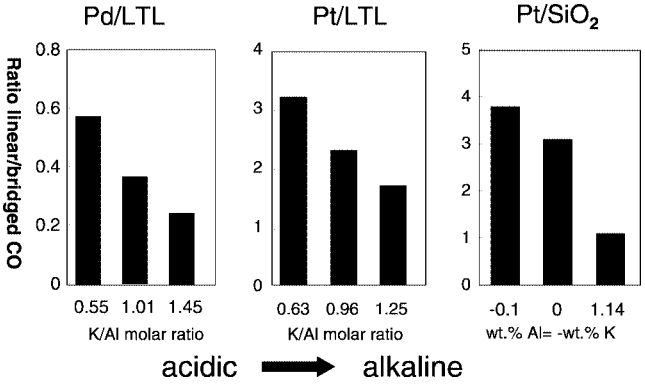

Figure 4. Ratio of linear to bridged CO in FTIR spectra as a function of the support alkalinity for Pd/LTL, Pt/LTL and Pt/SiO_2.

port alkalinity increases. Moreover, more importantly the ratio of the linear to bridge bonded CO is a strong function of the support alkalinity. This can be observed in figure 4, where the integrated intensity ratios of the linear to bridged bonded CO (L/B ratio) as calculated from the FTIR spectra is plotted for Pd/LTL, Pt/LTL and Pt/SiO_2 as a function of the support alkalinity. It can be seen that the L/B ratio decreases with increasing support alkalinity for all three catalyst series. The FTIR results of chemisorbed CO are a strong indication that the electronic structure of the catalytically active surface metal sites is influenced by the support. The L/B ratio systematically decreases for all catalysts with increasing alkalinity of the support.

3.3. Pt–H anti-bonding shape resonance

The Pt–H anti-bonding shape resonance was determined for three Pt/LTL samples with K/Al ratios of 0.63, 0.96 and 1.25, respectively. The EXAFS analysis [16] showed very small Pt particles with Pt–Pt co-ordination numbers around 4. For Pt particles dispersed in Y zeolite, the Pt–H anti-bonding shape resonance was obtained from specially prepared Pt/NaY and Pt/H-USY catalysts. HRTEM data collected on the EXAFS samples have shown that the Pt particles are dispersed inside the zeolite with a particle size distribution of 8–15 Å in diameter. This corresponds with an average Pt–Pt coordination number of 5.5 as obtained from the EXAFS data analysis [17]. Figure 5 shows, as a typical example, the normalised L_3 and L_2 edges for Pt/NaY after reduction (Pt–H) (solid line) and after evacuation (Pt) (dotted line). The energy scale in the figure is relative to the edge set at 0.6 times the step height of the Pt sample. The edges were aligned according to the procedure explained in [18]. It can be seen in figure 5 that chemisorption of hydrogen changes the shape and intensity of the near-edge spectra of both the L_2 ad the L_3 edges. The Pt–H shape resonance (AS) was isolated from the X-ray absorption near-edge spectra using the procedure as outlined and discussed in [18]. Figures 6 and 7 show the results obtained for the Pt/Y and Pt/LTL catalysts, respectively. Strong variations in both position and shape of the Pt–H shape resonance can be observed. This in turn implies that the electronic structure of the catalytically active metal surface sites strongly depend on the properties of the support. The AS data were fitted with the Fano profile in equation (1) using a modified expression for the phase

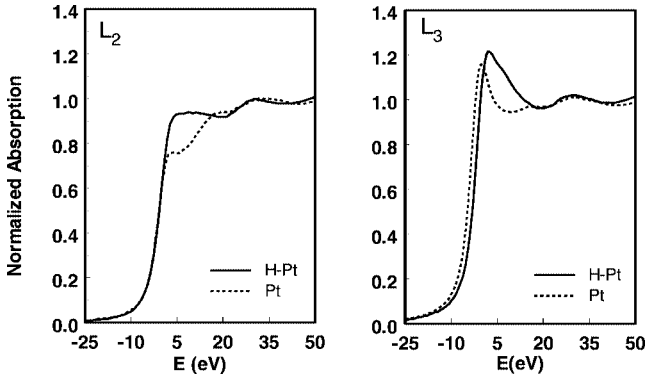

Figure 5. L_2 and L_3 X-ray absorption edges for Pt/NaY after reduction in H_2 (—) and after evacuation (· · ·).

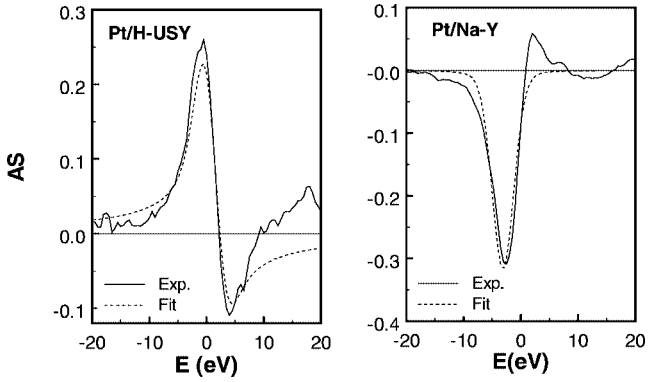

Figure 6. Pt–H anti-bonding shape resonance (AS) (—) and best fits (· · ·) using equation (1) for Pt/H-USY and Pt/NaY.

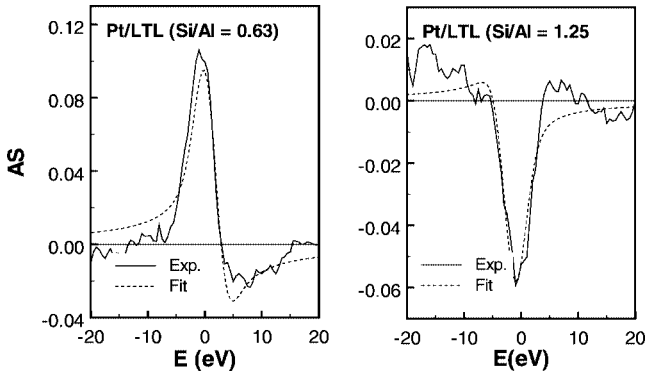

Figure 7. Pt–H anti-bonding shape resonance (AS) (—) and best fits (· · ·) using equation (1) for Pt/LTL(0.63) and Pt/LTL(1.25).

shift Φ [24]. The fits of the AS data are indicated in figures 6 and 7 with a dotted line. The optimum parameters from the fitting procedure are given in table 3.

4. Discussion

4.1. Neopentane hydrogenolysis

Neopentane cannot undergo a bifunctional mechanism because the neopentane molecule cannot form an alkene intermediate. Moreover, neopentane does not undergo protolytic cracking at the temperatures used for the catalytic reaction (250 °C). Therefore, the changes in the TOF cannot be ascribed to a bifunctional mechanism and are therefore only due to changes in the catalytic activity of the metal [27,28]. This is fully confirmed by the primary reaction products: methane, isobutane (hydrogenolysis) and isopentane (isomerisation).

Table 3
Fit parameters obtained from non-linear least squares fit of Fano profile to the hydrogen induced shape resonance in experimental spectra. Applied experimental width: Gaussian, 5 eV.

Catalyst	A (±0.03)[a]	E_{res}[b] (eV) (±0.3)	Width Γ (eV) (±0.4)	Φ[c] (calculated) (±0.1)
Pt/H-USY	1.58	0.9	0.6	0.6
Pt/NaY	1.71	−3.1	0.6	−1.6
Pt/LTL(0.63)	0.60	1.1	0.6	0.7
Pt/LTL(1.25)	0.26	−1.6	0.8	−1.1

[a] Relative to the L_2 absorption edge.
[b] Estimated uncertainty in each case.
[c] Equation (3) in [24] was used to determine Φ.

The neopentane hydrogenolysis results demonstrate that the TOF of Pd and Pt particles are strongly dependent on the support properties. The TOF decreases with increasing support alkalinity (K/Al ratio). The TOF increases with increasing number of protons, with increasing cation charge (Na^+ vs. La^{3+}) and with increasing Si/Al ratio and/or with the presence of extra-framework Al in the support. The trends are independent of the type of support; they are the same for microporous zeolites such as LTL and Y or macroporous supports such as SiO_2.

4.2. FTIR of chemisorbed CO

Both the linear and bridged CO adsorption bands shift to lower wavenumbers as the support alkalinity increases. Shifts in the CO band position are generally interpreted as evidence of changes in the electronic properties of supported metals. The exact position of the absorption bands depends on the catalysts parameters such as particle size [29], surface coverage [30] and electronic changes in the metal structure [31]. Since the particle sizes for a given catalyst series are not exactly the same and the bands are broad, the mere shifts in band position cannot be used as firm evidence for a change in electronic properties of the metal particles.

Theoretical calculations [32] have shown that the amount of bridged bonded CO increases at the expense of linearly coordinated CO when the binding energy of the metal electrons is located closer (i.e., at lower binding energy) to the binding energy of the $2\pi^*$ orbital of CO. The FTIR integrated intensity ratio of linear/bridged (L/R) bonded CO, therefore, is a direct measure of the difference in energy between the interacting d-orbitals and the $2\pi^*$ orbital of CO. Thus a smaller L/B ratio points to a lower binding energy of the interacting d-orbitals. It can be seen in figure 4 that the L/B ratio decreases with increasing support alkalinity Pd/LTL, Pt/LTL and Pt/SiO_2. From the results of the FTIR experiments, it can directly be concluded that an increasing

support alkalinity decreases the ionisation potential of the d-valence orbitals of the catalytically active surface metal sites.

4.3. Pt–H shape resonance

It is well known in the literature that hydrogen significantly affects the near-edge region of the Pt and Pd $L_{2,3}$ X-ray absorption edges. Mansour and Sayers [33] observed that the areas of the Pt $L_{2,3}$ white lines increased with exposure to H_2 in comparison to Pt foil and developed a quantitative technique for determination of the number of unoccupied d-electron states. Lytle et al. [34] observed significant changes in white line shape and intensity of the Pt $L_{2,3}$ edges for Pt/SiO_2 heated in H_2 vs. He and as a function of temperature. Samant and Boudart [35] noted similar changes in H–Pt vs. He/Pt clusters dispersed in Y zeolite. Asakura et al. [36] and Reifsnyder et al. [37] suggested a new Pt–H resonance state visible in XAFS data after hydrogen adsorption on supported Pt particles. Finally, Boyanov et al. [38] observed two features in the H/Pt minus Pt foil $L_{2,3}$ difference spectra of Pt clusters supported on zeolite Y and interpreted them as spin–orbit doublets.

The analysis method used in this study is different in two aspects from procedures reported in the literature: namely (i) the edge alignment and (ii) the choice of reference spectrum, as fully discussed in [18]. In the literature studies mentioned above, either raw data were directly subtracted from each other, or all edges were aligned with the $L_{2,3}$ edges of platinum foil before subtraction. The use of platinum foil as the reference introduces both electronic and geometric contributions in the difference spectra due to the broader d-band and higher Pt–Pt coordination number of bulk platinum. Using the spectrum of the clean Pt-cluster as a reference minimises the unwanted contributions in the spectra. The alignment procedure used in this work, based upon the absence (L_2) or presence (L_3) of electronic structure (AS state), is critical to the success of the method. This alignment procedure is particularly suitable to study systems where much larger chemical shifts (initial state effects) are expected (e.g., large promoter and metal–support effects).

By using this alignment procedure it was possible to isolate the Pt–H anti-bonding state shape resonance. The parameters describing the AS shape resonance are tabulated in table 3. The fit parameters differ somewhat from the values given previously [17,39]. This is due to the fact that a different (more optimised) expression was used for the phase shift Φ. However, the trends found in the values for E_{res} are the same. It can be seen that the difference in energy of the Pt–H anti-bonding state and the Fermi level (E_{res}) of the Pt/LTL catalysts decreases with increasing alkalinity of the LTL support. A higher Si/Al ratio and/or the presence of extra-framework Al in Y zeolite also influence the position of the Pt–H anti-bonding state. The Pt–H anti-bonding state in Pt/H-USY has a larger value of E_{res} than for Pt/NaY, showing also an influence of the Si/Al ratio of the zeolite framework and/or the type of cations present. The difference in values of E_{res} as a function of the difference in support properties indicates a direct influence of the support on the electronic structure of the supported metal particles.

4.4. Mechanism of the metal–support interaction and Pt–H bond strength

The Pt–CO FTIR data and Pt–H shape resonance data provide direct evidence that the support composition leads to a change in the energy of the metal valence orbitals and a difference in Pt–adsorbate bonding. However, these techniques do not give information about the mechanism by which the support alters the electronic properties of the metal particles. Insight into the origin of the metal–support interaction, however, can be obtained from recent atomic XAFS (AXAFS) studies on Pt particles dispersed in LTL and Y zeolite [16,17]. AXAFS arises from scattering off the *deeper localised* valence band electrons of the absorbing atom itself. The position and shape of the Fourier transform AXAFS peak is related to the difference between the free atom potential and the interatomic metal potential. The interatomic potential of the platinum atoms close to the support will be most strongly influenced by nearby atoms, which are the oxide ions of the support as shown by EXAFS analysis. The Coulomb potential field of the support oxygen ions will extend to the metal and will lead to a change in the shape of the metal atomic potential. By increasing the negative charge on the support oxygen (as in alkaline supports) the interatomic potential between platinum and oxygen will change leading to a shift of the valence d-orbitals to lower binding energy.

It is now possible to understand the influence of the different support properties on the electronic structure of the catalytically active metal surface sites. The influence of the Coulomb potential field of the support oxygen ions is averaged over the whole particle and therefore is also felt by the surface metal atoms. Adding potassium to the LTL support increases the alkalinity of the support and therefore leads to a small increase (δ^-) in the negative charge of the support oxygen ions. The position of the valence d-orbitals of the metal particles moves to lower binding energy. This fully explains the FTIR results of the chemisorbed CO; a decrease in the L/B ratio is observed.

An increase in the number of protons increases the acidity of the support, leading to a small decrease (δ^+) in the negative charge of the support oxygens. Recent detailed ^{27}Al MQ MAS studies [40] revealed the similarity in polarisation behaviour of La^{3+} and extra-framework Al^{3+}, the latter present in HUSY due to the steaming treatment. The polarisation by La^{3+} and extra-framework Al^{3+} of the zeolite Y framework will also lead to a small decrease (δ^+) in the negative charge of the support oxygen ions. XPS studies and calculation of the Madelung potential in zeolites [41] show that the charge on the zeolite oxygens strongly depends on the Si/Al ratio of the zeolite and polarisation power of the cations as determined by their electronegativity. XPS results

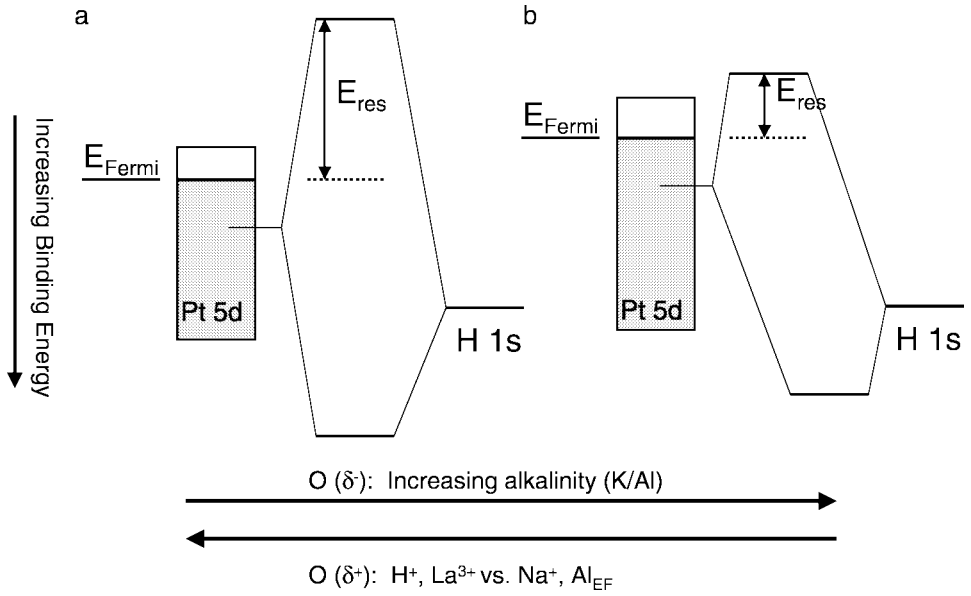

Figure 8. Schematic representation of the Pt–H bonding as a function of the support properties.

revealed that more acidic zeolites show higher binding energy for the oxygen atoms, pointing to less negative O atoms and more negative Madelung potentials [41].

The influence of the support properties on the catalytic behaviour of the surface metal atoms can be understood by examining the change in the Pt–H bonding. This is schematically illustrated in figure 8. As the alkalinity of the LTL support increases with increasing K/Al ratio, the negative charge on the support oxygen ions increases by an amount δ^-. This induces a shift of the interacting d-orbitals to lower binding energy (i.e., decrease in ionisation potential). The energy position of the interacting H 1s orbital stays the same. The difference in energy of the Pt–H anti-bonding state with respect to the Fermi level (E_{res}) decreases, as is derived from the analysis of the shape resonance. Combining these results, as presented in this paper (experimentally obtained from Pt–CO FTIR and Pt–H shape resonance data), with the AXAFS data presented in [16,17] shows that the Pt–H bond strength decreases with increasing alkalinity of the support (increasing K/Al ratio). In contrast, increasing the number of protons, the charge of the cations (La^{3+} versus Na^+) and the presence of extra-framework Al results in a decrease of the negative charge by an amount δ^+. The interacting d-orbitals of the surface metal atoms shifts to higher binding energy (i.e., increase in ionisation potential) with a simultaneous increase in the value of E_{res}. This leads to an increase in the Pt–H bond strength.

The change in Pt–H bonding as a function of the support properties has to be further correlated to the change in the TOF of neopentane hydrogenolysis. Preliminary results on saturation reactions of aromatics are showing the same trends with the support properties as found for the hydrogenolysis of neopentane. Therefore, we believe that the mechanism of the metal–support interaction as outlined in this paper is of more general validity.

5. Summary

This paper demonstrates that the energy and spectral lineshape of the Pt–H resonance vary systematically with support properties such as alkalinity, number of protons, charge of cations and the presence of extra-framework Al. The FTIR studies on chemisorbed CO are fully in line with the results of the Pt–H shape resonance. The mechanism of the metal–support interaction that affects the electronic properties of the surface metal atoms in metal–supported catalysts, and in turn changes their catalytic activity, has been elucidated. The proposed mechanism is indicated not only by (i) the Pt–CO FTIR data and the Pt–H anti-bonding shape resonance data as summarised in this paper, but also by (ii) the results of AXAFS studies recently published in the literature. The mechanism is based upon a direct influence of the Coulomb field induced by the support oxygen ions on the position in energy of the metal valence d-orbitals.

References

[1] R.A. Della Betta and M. Boudart, in: *Proc. 5th Int. Congr. Catal.*, ed. J.W. Hightower (North Holland, Amsterdam, 1973) p. 1329.
[2] G. Larsen and G. L. Haller, Catal. Lett. 3 (1989) 103.
[3] A. de Mallmann and D. Barthomeuf, J. Chim. Phys. 87 (1990) 535.
[4] S.T. Homeyer, Z. Karpinski and W.M.H. Sachtler, J. Catal. 123 (1990) 60.
[5] W.M.H. Sachtler and A.Y. Stakheev, Catal. Today 12 (1992) 283.
[6] D.L. Shawn and M.A. Vannice, J. Catal. 143 (1993) 539.
[7] D.L. Shawn and M.A. Vannice, J. Catal. 143 (1993) 554.
[8] B.L. Mojet, M.J. Kappers, J.T. Miller and D.C. Koningsberger, in: *11th Int. Congr. Catal.*, Stud. Surf. Sci. Catal. Vol. 101B, eds. J.W. Hightower, W.N. Delgass, E. Iglesia and A.T. Bell (Elsevier, Amsterdam, 1996) p. 1165.
[9] Z. Zhang, T.T. Wong and W.M.H. Sachtler, J. Catal. 128 (1991) 131.
[10] A.Y. Stakheev and W.M.H. Sachtler, J. Chem. Soc. Faraday Trans. 87 (1991) 3703.
[11] G. Larsen and G.L. Haller, Catal. Today 15 (1992) 431.

[12] A. de Mallmann and D. Barthomeuf, J. Chem. Phys. 87 (1990) 535.
[13] A. de Mallmann and D. Barthomeuf, Stud. Surf. Sci. Catal. 46 (1989) 429.
[14] A.P.J. Jansen and R.A. van Santen, J. Phys. Chem. 94 (1990) 6764.
[15] E. Sanchez-Marcos, A.P.J. Jansen and R.A. van Santen, Chem. Phys. Lett. 167 (1990) 399.
[16] B.L. Mojet, J.T. Miller, D.E. Ramaker and D.C. Koningsberger, J. Catal. 186 (1999) 373.
[17] D.C. Koningsberger, J. de Graaf, B.L. Mojet, D.E. Ramaker and J.T. Miller, Appl. Catal. 191 (2000) 205.
[18] D.E. Ramaker, B.L. Mojet, M.T. Garriga Oostenbrink, J.T. Miller and D.C. Koningsberger, J. Phys. Chem. Chem. Phys. 1 (1999) 2293.
[19] N.A. Bhore, M.T. Klein and K.B. Bischoff, Ind. Eng. Chem. Res. 29 (1990) 313.
[20] M.J. Kappers, M. Vaarkamp, J.T. Miller, F.S. Modica, M.K. Barr, J.H. van der Maas and D.C. Koningsberger, Catal. Lett. 21 (1993) 235.
[21] M. Vaarkamp, B.L. Mojet, F.S. Modica, J.T. Miller and D.C. Koningsberger, J. Phys. Chem. 99 (1995) 16067.
[22] J.W. Cook and D.E. Sayers, J. Appl. Phys. 52 (1981) 5024.
[23] B. Hammer and J.K. Nørskov, Nature 376 (1995) 238.
[24] D.C. Koningsberger, M.K. Oudenhuijzen, J.H. Bitter and D.E. Ramaker, Topics Catal. 10 (2000) 167.
[25] B.L. Mojet, M.J. Kappers, J.T. Miller and D.C. Koningsberger, Stud. Surf. Sci. Catal. 101 (1996) 1165.
[26] B.L. Mojet, M.J. Kappers, J.C. Muijsers, J.W. Niemantsverdriet, J.T. Miller, F.S. Modica and D.C. Koningsberger, Stud. Surf. Sci. Catal. 84 (1994) 909.
[27] S.M. Davis and G.A. Somorjai, in: *The Chemical Physiscs of Solid Surfaces and Heterogeneous Catalysts*, Vol. 4, eds. D.A. King and D.P. Woodruff (Elsevier, Amsterdam, 1982) p. 271.
[28] J.R. Anderson and N.R. Avery, J. Catal. 16 (1967) 315.
[29] R. van Hardeveld and F. Hartog, Adv. Catal. 22 (1972) 75.
[30] F. Stoop, F.J.C.M. Toolenaar and V. Ponec, J. Catal. 73 (1982) 50.
[31] G. Blyholder, J. Phys. Chem. 68 (1964) 2772.
[32] R.A. van Santen, J. Chem. Soc. Faraday Trans. I 83 (1987) 1915.
[33] A.N. Mansour, J.W. Cook, Jr. and D.E. Sayers, J. Phys. Chem. 96 (1992) 4690.
[34] F.W. Lytle, R.B. Greegor, E.C. Marques, V.A. Biebesheimer, D.R. Sandstrom, J.A. Horsley, G.H. Via and J.H. Sinfelt, ACS Symp. Ser. 288 (1985) 280.
[35] M.G. Samant and M. Boudart, J. Phys. Chem. 95 (1991) 4070.
[36] K. Asakura, T. Kubota, N. Ichikuni and Y. Iwasawa, Stud. Surf. Sci. Catal. 101 (1996) 911.
[37] S.N. Reifsnyder, M.M. Otten, D.E. Sayers and H.H. Lamb, J. Phys. Chem. B 101 (1997) 4972.
[38] B.I. Boyanov and T.I. Morrison, J. Phys. Chem. 100 (1996) 16318.
[39] B.L. Mojet, D.E. Ramaker, J.T. Miller and D.C. Koningsberger, Catal. Lett. 62 (1999) 15.
[40] J.A. van Bokhoven, A.L. Roest, J.T. Miller, G.H. Nachtegaal, A.P.M. Kentgens and D.C. Koningsberger, J. Phys. Chem., in print.
[41] W. Grünert, M. Muhler, K.P. Schröder, J. Sauer and R. Schlögl, J. Phys. Chem. 98 (1994) 10920.